

Depth-aware Glass Surface Detection with Cross-modal Context Mining

Jiaying Lin* Yuen Hei Yeung* Rynson W.H. Lau†

Abstract—Glass surfaces are becoming increasingly ubiquitous as modern buildings tend to use a lot of glass panels. This however poses substantial challenges on the operations of autonomous systems such as robots, self-driving cars and drones, as the glass panels can become transparent obstacles to the navigation. Existing works attempt to exploit various cues, including glass boundary context or reflections, as a prior. However, they are all based on input RGB images. We observe that the transmission of 3D depth sensor light through glass surfaces often produces blank regions in the depth maps, which can offer additional insights to complement the RGB image features for glass surface detection. In this paper, we propose a novel framework for glass surface detection by incorporating RGB-D information, with two novel modules: (1) a cross-modal context mining (CCM) module to adaptively learn individual and mutual context features from RGB and depth information, and (2) a depth-missing aware attention (DAA) module to explicitly exploit spatial locations where missing depths occur to help detect the presence of glass surfaces. In addition, we propose a large-scale RGB-D glass surface detection dataset, called *RGB-D GSD*, for RGB-D glass surface detection. Our dataset comprises 3,009 real-world RGB-D glass surface images with precise annotations. Extensive experimental results show that our proposed model outperforms state-of-the-art methods.

Index Terms—RGB-D glass surface detection, Glass surface detection, Multi-modal learning.

1 INTRODUCTION

ALTHOUGH majority of the objects that we see in our daily life exhibit distinctive optical characteristics, glass surfaces, however, typically do not possess any distinctive visual properties. Their contents are essentially represented by the contents behind them. This makes it difficult for existing computer vision systems to detect them. On the other hand, modern architects/designers tend to use a lot of glass panels in their designs, and glass surfaces are becoming ubiquitous. They appear in both indoor and outdoor environments as, *e.g.*, glass doors/windows, shop windows, and glass walls. It is therefore critical to be able to detect glass surfaces accurately, in order to deploy autonomous machines such as robots and drones safely.

Early studies on glass surface detection try to leverage priors, *e.g.*, visual cues [40]. Later on, rich sensor data is incorporated, including laser sensor [65], [76] and LiDAR sensor [56], [92], for computations using point clouds and object mapping. A recent method [69] uses fiducial markers to help identify the presence of mirror and glass surfaces, but requires special hardware for tagging. Later on, the potential of deep learning models were first leveraged by [41] and [31]. Most recently, EBLNet [16] is proposed for glass surface detection through enhanced boundary learning on glass surfaces. However, since EBLNet is a RGB-based method and relies heavily on boundary learning, it may fail if the boundaries of glass surfaces are ambiguous

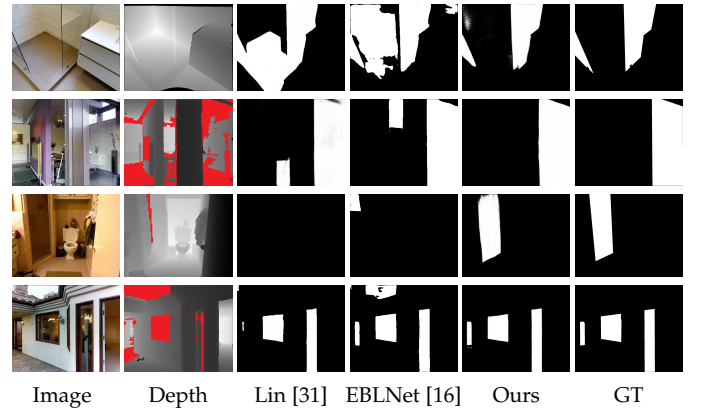


Fig. 1. The advantages of detecting glass surfaces with RGB-D images. The first row shows that the depth map can provide a strong cue for glass surface detection. State-of-the-art methods, Lin *et al.* [31] and EBLNet [16] relying only on input RGB images are not able to correctly separate the glass surfaces from the background. Based on learning the cross-modal contexts, our proposed model can detect the glass surfaces accurately. The second, third and fourth rows show three very challenging scenes with glass surfaces, where the glass surfaces may not be easily identified even for humans. State-of-the-art methods either over- or under-detect the glass surfaces. Through learning the cross-modal contexts and the correlation between depth-missing regions and glass surface regions, our proposed model can detect the glass surfaces accurately in all three scenes. Note that red regions in the depth images represent missing depths.

or there are some distracting glass-like regions in the input image.

Fig. 1 shows some challenging scenarios where state-of-the-art RGB-based glass surface detection methods, Lin *et al.* [31] and EBLNet [16], fail. In the first row, both Lin *et al.* [31] and EBLNet [16] are confused by the similarity between the

• J. Lin, Y.H. Yeung and R.W.H. Lau are with the Department of Computer Science, City University of Hong Kong, HKSAR, China. E-mail: jiajinlin5-c@my.cityu.edu.hk, yh.y@my.cityu.edu.hk, Rynson.Lau@cityu.edu.hk.

* Jiaying Lin and Yuen Hei Yeung are joint first authors.

† Rynson W.H. Lau is the corresponding author.

glass regions and the tiles in the shower area, and consider some of the tiles as glass regions. The second to fourth rows show three challenging scenes, where the glass surfaces may not be easily identified even by humans. Lin *et al.* [31] and EBLNet [16] either over- or under-detect the glass regions. In particular, in the second row, the appearance of the room entrance in the middle is very similar to the glass wall of the room on the right hand side. Both state-of-the-art methods partially mis-detect it as glass regions.

In this paper, we aim to address the limitation of RGB-based glass surface detection methods that they heavily rely on boundary learning, causing them to fail if the glass boundaries are ambiguous or there are glass-like regions in the image. We address this problem from a depth-aware perspective. Our key observation is that compared with the *correct* depth of a glass surface, the *captured* depth of it by a depth sensor typically has two properties, due to the transmission and possibly reflection of the glass surface: 1) the captured depth is noisier, and 2) missing depths frequently appear around the surface. These two properties indicate that glass surfaces have different contextual characteristic representation in the depth map, compared with that of the RGB image. Our insight from this observation is that cross-modal context and spatial information of missing depths can provide strong cues for glass surface detection. This motivates us to design a novel depth-aware glass surface detection method with two new modules: a cross-modal context mining (CCM) module to adaptively fuse multi-modal data by utilizing depth scans coupled with RGB data, and a depth-missing aware attention (DAA) module to explicitly learn the correlations between missing depths and glass regions.

In order to train our model, we need to have a RGB-D dataset on transparent surfaces. Although there is RGB-D dataset [52] available for transparent object detection, it is not suitable for our purpose for two reasons. First, the aim of this dataset is to localize small transparent objects with limited patterns of shapes and object types, while we focus on a more challenging task that detecting glass surfaces without well-defined shapes. Second, it contains only 440 RGB-D images captured from a single scene with four object types (*i.e.*, beer mugs, water glasses, white beer glasses, and wine glasses), making it difficult to generalize to real-world applications. To address these limitations, we construct a new large-scale RGB-D glass surface dataset from diverse scenes with glass surfaces. Our dataset contains a total of 3,009 RGB-D images that include glass surfaces with corresponding annotated masks. A dataset of this scale allows robust model training and evaluation. We have conducted extensive experiments to evaluate our method, in comparison with the state-of-the-art methods from the relevant areas, and show that the proposed model outperforms existing methods on our proposed dataset. We will release our RGB-D dataset and codes to the public to facilitate further research.

Our contributions can be summarised as follows:

- 1) We proposed a framework for glass surface detection by incorporating the depth information, with two novel modules: a cross-modal context mining (CCM) module to jointly learn the RGB context

features and depth context features for comprehensive RGB-D context modeling, and a depth-missing aware attention (DAA) module to explicitly exploit the location where the depth information is missing in the depth maps for glass surface detection.

- 2) We constructed a challenging and large-scale glass surface dataset of 3,009 images from diverse real-world scenes, coupled with corresponding depth maps and ground truth annotations.
- 3) Extensive experimental results demonstrate the superior performances of our proposed method over state-of-the-art methods.

2 RELATED WORK

2.1 Glass Surface Detection

Early methods on glass surface detection are mainly based on hand-craft features. As LiDAR is not able to capture signals from specular surfaces, *e.g.*, glass surfaces, at most angles, Foster *et al.* [12] propose refinement on an occupancy-grid algorithm to distill glass object surfaces. In view of the inability of LiDAR sensors to properly trace transparent surfaces, ultrasonic scans are incorporated in [66], [67], along with fusion on depth scans [18], [67]. These heuristic approaches require various kinds of sensors and hand-craft features, and do not take advantages of the deep-learning technologies, resulting in unsatisfactory performances.

With the popularity of deep learning, Mei *et al.* [41] propose the first deep-learning model for detecting glass surfaces, given just an RGB image. This method does not require any special hardware. As this model relies heavily on contextual contrast learning, it likely fails in complex scenes with insufficient contexts. Lin *et al.* [31] extend contextual contrast learning with modules for detecting glass boundaries and reflections. However, if the glass surfaces lack reflections or have ambiguous boundaries, the model may not be able to detect the glass surfaces correctly. Similar to [31], He *et al.* [16] propose EBLNet for glass surface detection based on learning the glass boundaries. However, all these deep-learning based methods only consider the RGB information for glass surface detection, and can easily be confused by the distracting glass-like regions that look like glass surfaces, *e.g.*, a door frame. In contrast, we propose in this paper a multi-modal glass surface detection method, based on using RGB-D images as input. Our experimental results show that the proposed method is more robustness and accurate.

2.2 Transparent Object Detection

Compared with glass surface detection, research on transparent object detection (TOD) focuses on detecting small transparent objects, such as wine glass and glass balls, which typically have well-defined shapes or boundary properties. Adelson and An [2] study the optical characteristics of transparency. Murase [42] studies image pattern distortion of moving an object behind a transparent layer by leveraging optical flow. Hata *et al.* [15] and Wang *et al.* [60] try to extract the shapes of transparent objects, while Fritz *et al.* [13] study the local patch structure of transparent objects. With a wider availability of hardware, some recent TOD methods

integrate more accurate measurement data, including data from light-field sensors [75] and from infra-red sensors [14], [53]. Some latest deep learning based TOD methods use auxiliary information, including polarization [23] and specular reflection [19], to assist the detection. Other methods use explicit boundary maps [72] for training, or a transformer architecture [73], [81] for improved performances. However, while the former induces additional data preparation and computation costs, the latter further abstracts the object representations with feature embedding dictionary and has a constrained set of prototype categories.

In general, transparent objects are small objects, and tend to have different lighting properties along the boundary. Hence, most TOD methods exploit the boundary cue or some auxiliary information to achieve good performances. However, glass surfaces generally do not possess these properties, making these TOD methods not suitable for detecting glass surfaces.

2.3 Salient Object Detection

There are many salient object detection methods proposed [62]. Most models utilise multi-scale and feature level structures [29], [30], [37], [44], [63], [82], [84], [89] to comprehensively capture local and global representations from the image. In order to retain information from early levels, skip connections [6], [17], [38], [59], [68], [70] are introduced. To guarantee the prediction accuracy, recurrence is applied for more iterations [34], [58]. Further, to abstract and generalise the underlying low-level and high-level features better, the encoder-decoder structure [7], [26], [85] and feature pyramid network [33], [57], [64], [90] are adopted in recent works for salient object detection. To guide the model to focus on context- and boundary-specific details, contextual attention [35], [61], [86], [87] and boundary-aware modules [11], [48] are formulated.

With the use of depth images, attempts are first started with priors, *e.g.*, region contrast, background, and orientation priors [51], [88]. Qu *et al.* [50] further suggest integrating the prior information into CNNs, which achieves significant performance improvement. As deep learning techniques become popular, object feature learning turns into fully convolutional operations, rather than based on hand-crafted features and pre-defined priors. The focus is then shifted over to the fusion process of multi-modal data [5], [10], [28], [47], [79], [95], and later incorporating the attention mechanism [21], [27], [36], [55], [83], [93] and recurrence [46] to further promote feature integration. One recent approach [78] creatively adopt conditional variational auto-encoder to model the uncertainty in latent variable.

The visual appearance of glass surfaces depends mainly on the objects appearing behind them, instead of the glass surfaces themselves. Hence, existing salient object, which detect local object saliency, are not suitable for detecting glass surfaces.

3 RGB-D GSD DATASET

There are many existing datasets [3], [4], [9], [20], [39], [43], [54] that incorporate depth information, for other tasks such as semantic segmentation and salient object detection.

For glass surface detection, there are two existing datasets available [41] and [31]. However, they do not include depth information. In order to train our model and to encourage further research, we propose an RGB-D Glass Surface Detection (RGB-D GSD) dataset here.

Dataset construction. This dataset is an attentively curated ensemble of three existing datasets originally developed for scene understanding, including SUN RGB-D [3], 2D-3D-Semantics [54] and Matterport3D [4]. It contains a total of 3,009 images, providing a large extent of categorical diversity of glass surfaces such as window, door, wall, table, cabinet and guardrail. We follow the dataset split of the original [datasets](#). For SUN RGB-D [3], we have identified 630 images from the training set and 573 images from the test set of the original dataset, with glass surfaces. We then reallocate 290 images from the test set to the training set in order to keep the training-test ratio. For 2D-3D-Semantics [54], we follow cross validation fold #2 (*i.e.*, areas 1, 5, 6 for training and areas 2, 4 for testing). For Matterport3D [4], we randomly split the selected images into a training set with 992 images and a test set with 214 images. Refer to Table 1 for a summary of the composition of our dataset. Each RGB image is accompanied with a pre-processed depth image and finely annotated ground truth mask. The depth images were taken by different RGB-D cameras models, *e.g.*, Asus Xtion, Kinect v2 [3] and Matterport [4] cameras. Although all depth images were encoded in 16-bit grayscale format, the definitions for missing depth are not the same in these three original datasets. For example, in SUN RGB-D [3], un-returned depth signals were set to be the minimum value, which depends on the the depth ranges of individual images. On the other hand, 2D-3D-Semantics [54] assumed invalid depth signals to be the maximum depth value (*i.e.*, $2^{16} - 1$).

For these datasets to be consistent, we normalize all depth images to the range $[0, 2^{16} - 1]$, and set all invalid depth values to be the minimum value (*i.e.*, 0). In addition, as these datasets do not aim at labelling glass surfaces, they contain inaccurate glass surface labels. For example, the objects inside a glass surface instead of the glass surface itself were labelled; handles, frames or blinds were labelled as part of the glass surface. Hence, we use Labelme¹ to manually relabel the glass surfaces in these images. Figure 2 shows some examples from our RGB-D GSD dataset.

TABLE 1

Composition of our proposed RGB-D GSD dataset. We collect glass images from three existing RGB-D datasets. Note that as these datasets were originally created for other tasks, they do not include accurate annotations of glass surface masks. Thus, we annotate the GT masks of the glass surfaces in our dataset construction.

Dataset	Whole	Train	Test
SUN RGB-D [3]	1,203	920	283
2D-3D-Semantics [54]	600	488	112
Matterport3D [4]	1,206	992	214
Total	3,009	2,400	609

Dataset analysis. We analyse the datasets with the following statistical metrics:

1. <https://github.com/wkentaro/labelme>



Fig. 2. Examples from our RGB-D GSD dataset. Top, middle and bottom rows show RGB images, depth maps, and GT glass surface masks overlaid on the RGB images, respectively.

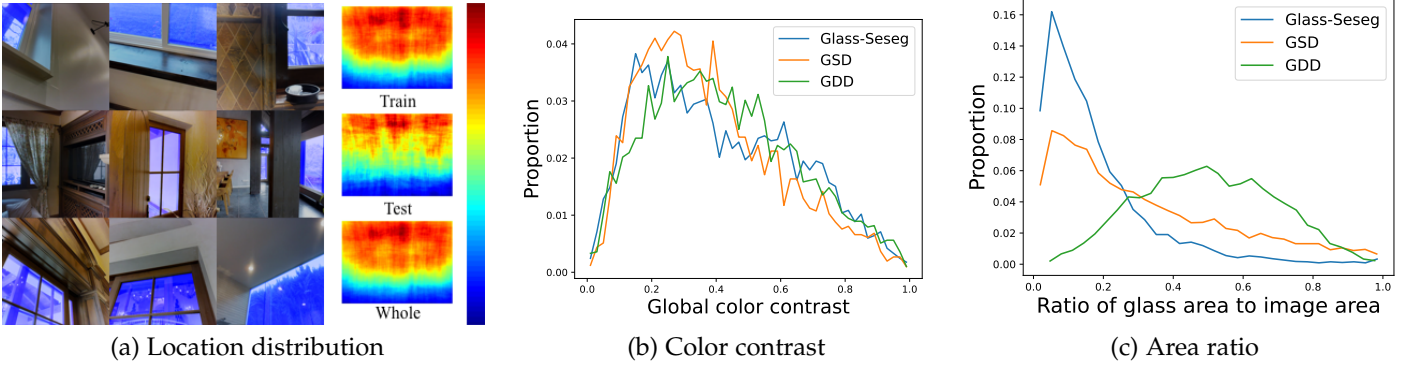


Fig. 3. Statistics of our proposed dataset.

- **Glass Location.** The glass location distribution is the average of all glass surface regions in the dataset. The maps in Figure 3(a) show that glass surfaces mainly concentrate at the top region, which is consistent in the training and testing splits. This also avoids the “center bias” problem due to natural observation tendency.
- **Color Contrast.** The color contrast between glass and non-glass regions should ideally be low. Otherwise, salient color features can skew the glass surface detection task. We measure the color contrast by computing the χ^2 distance of the RGB histograms between glass and non-glass regions. Figure 3(b) compares the color contrast among GDD [41], GSD [31] and our RGB-D GSD. In general, the contrast values of our RGB-D GSD images concentrate in the lower quartile ($0 < \text{contrast} < 0.4$), which is similar to the other two datasets.
- **Area Ratio.** This metric is defined as the size of the glass region over the size of the image. This illustrates the level of semantic context that the images provide. In other words, a smaller glass region leaves more room for the surrounding environment to offer additional hints. As mentioned in [31], GDD [41] contains primarily close-up shots, which limits the amount of contextual information. In addition, in real-life scenario, an autonomous system is expected to be able to detect objects and perform scene understanding tasks as early as possible. Therefore, having data of low area ratio is much more meaningful and

beneficial for model training. As demonstrated in Figure 3(c), RGB-D GSD has more images with small glass areas than the other datasets.

4 METHOD

Fig. 4 shows the architecture of our proposed framework for RGB-D glass surface detection. The proposed framework consists of four major components: the backbone network for the input RGB images (in red), the backbone network for the input depth maps (in yellow), the cross-modal context mining (CCM) modules (in blue), and the depth-missing aware attention (DAA) modules (in green). These components are arranged to enable multi-stage feature learning with bottom-up and top-down information flows.

In our framework, we first feed the input RGB image to the backbone network [74] to extract multi-scale RGB backbone features. Specially, we only use the outputs from the last four stages of the backbone network [74], *i.e.*, *conv1*, *conv2*, *conv3*, and *conv4*, as our RGB backbone features.

Unlike the RGB images, we adopt a different backbone network to extract depth features from the input depth map, as shown in Table 2. The depth backbone network that we use is much simpler and lighter, compared to the RGB one. There are two reasons. First, using a lighter depth backbone network makes our full framework more efficient in both training and test stages. Second, we observe that depth maps contain sparser information. Simply adopting the same backbone network as the RGB image for the depth map may cause a modality gap between the RGB and depth information, which will lead to performance degradation.

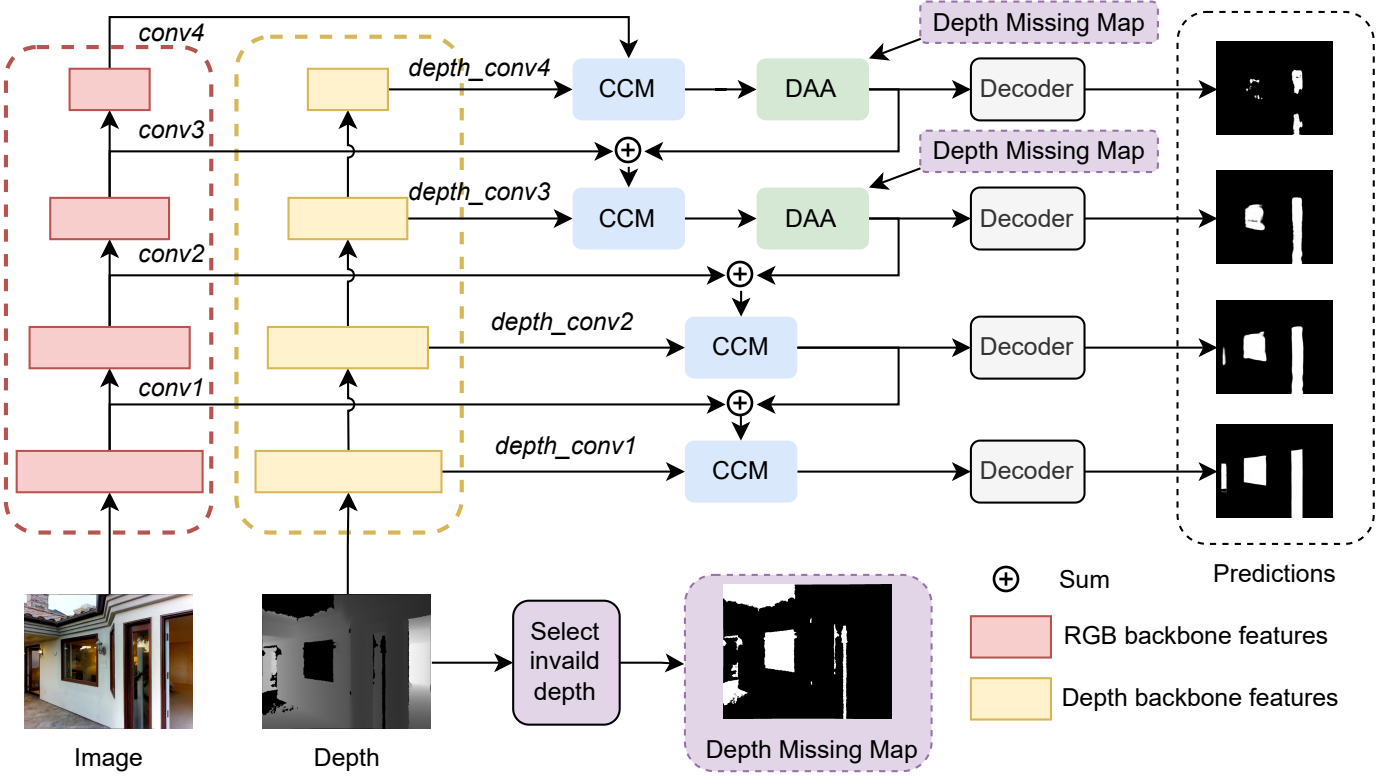


Fig. 4. The pipeline of our proposed framework. Given an input image and a corresponding depth map, our method first extracts multi-scale image features and depth features with a RGB backbone network [74] and a depth backbone network shown in Table 2. It then uses a novel CCM module (blue blocks) in each stage to learn cross-modal contextual features. For cross-modal contextual features in *stage4* and *stage3*, it further uses a DAA module (green blocks) to enhance them by exploiting the spatial information of the missing depths. Finally, it uses a decoder to extract the prediction of glass surfaces at each scale.

TABLE 2

The architecture of the depth backbone network that we use for the input depth map. It consists of five stages, and each stage contains a convolution layer followed by a pooling layer. Note that each “conv-BR” corresponds a sequence of convolution layer, BatchNorm layer and ReLU activation. K , S and P denote the number of kernels, the number of strides and the padding size, respectively, used in the convolution layer.

Layers Name	Layer Details	Output Size
Convolution Pooling	3×3 conv-BR, $K = 8$, $S = 1$, $P = 1$ 2×2 max pool, stride 2	384×384 192×192
Convolution Pooling	3×3 conv-BR, $K = 16$, $S = 1$, $P = 1$ 2×2 max pool, stride 2	192×192 96×96
Convolution Pooling	3×3 conv-BR, $K = 32$, $S = 1$, $P = 1$ 2×2 max pool, stride 2	96×96 48×48
Convolution Pooling	3×3 conv-BR, $K = 64$, $S = 1$, $P = 1$ 2×2 max pool, stride 2	48×48 24×24
Convolution Pooling	3×3 conv-BR, $K = 128$, $S = 1$, $P = 1$ 2×2 max pool, stride 2	24×24 12×12

Similar to the RGB backbone network, we only use the outputs from the last four stages, denoted as *depth_conv1*, *depth_conv2*, *depth_conv3*, and *depth_conv4*.

After obtaining the RGB backbone features and the depth backbone features, we first feed the uppermost RGB and depth backbone features (*i.e.*, *conv4* and *depth_conv4*) into a CCM module to capture the multi-modal contextual

features comprehensively at the latest stage (*i.e.*, *stage4*). To obtain the depth-missing map for the DAA module, we construct a binary depth-missing map from the input depth map by setting the invalid depth pixels to 1’s and valid depth pixels to 0’s. The output multi-modal contextual features from the CCM module and the resized depth-missing map are then fed into the DAA module to enhance the extracted multi-modal contextual features by exploiting the spatial location information where missing depths occur. Finally, the decoder takes the enhanced contextual features as input and produces a coarse binary mask representing the detected glass surfaces of *stage4*.

The enhanced contextual features from *stage4* are then added to the RGB backbone features (*i.e.*, *conv3*) of the preceding stage (*i.e.*, *stage3*), before feeding into a CCM module, a DAA module, and finally, a decoder. This process is repeated in *stage2* and *stage1*, except that we remove the depth missing attention in these two early stages for two reasons. First, the depth-missing map that we use indicates spatial locations where depths are missing. While such spatial information can be learnt from the upper layers (*i.e.*, later stages) easily, it is much harder to learn from the lower layers (*i.e.*, earlier stages). Thus, we apply the DAA module in the two upper layers to allow our framework to exploit low- and high-level information effectively. Second, as the spatial size of the features increases from the later stages to the earlier stages, adopting additional components to the early stages will heavily decrease the efficiency of the

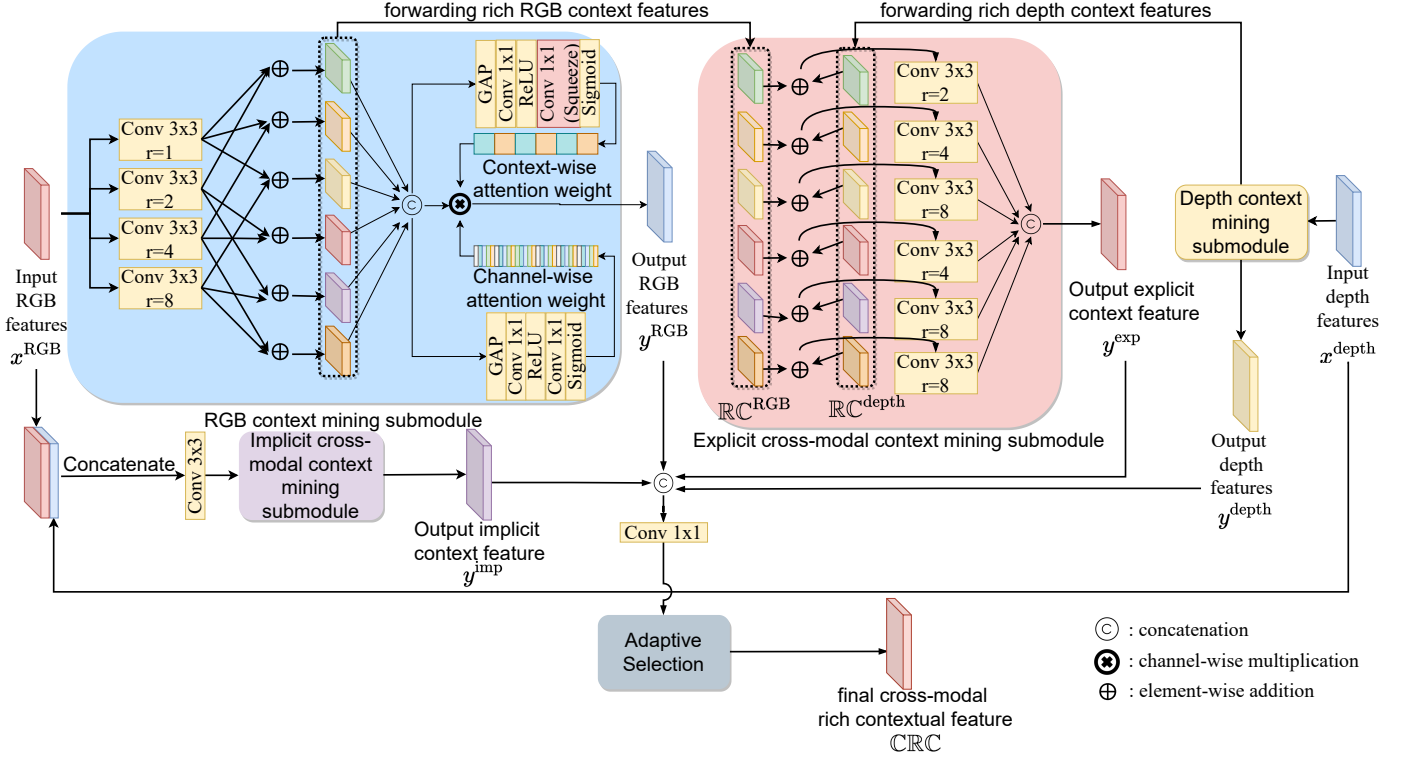


Fig. 5. Illustration of our proposed cross-modal context mining (CCM) module. It consists of four submodules: a RGB context mining submodule, a depth context mining submodule, an implicit multi-modal context mining submodule, and an explicit multi-modal context mining submodule. The CCM module first takes the RGB and depth features as input and outputs intermediate contextual features with its four submodules. These intermediate features are then concatenated and adaptively selected to generate the final cross-modal rich context features as the output of the CCM module.

proposed network.

Based on the above progressive refinement process, the decoder in the earliest stage (*i.e.*, *stage1*) outputs the finest binary mask as the output prediction of our framework.

For the rest of this section, we first discuss how the proposed CCM module exploits multi-modal contextual features to adaptively learn individual and mutual context features in Section 4.1, and how the proposed DAA module takes advantage of the depth-missing information to help detect glass surfaces in Section 4.2. We then describe the loss functions that we use to train the whole framework.

4.1 Cross-modal Context Mining (CCM) Module

Previous works [31], [41] on glass surface detection show that contextual information is very useful for the task. However, these works focus only on single-modal glass surface detection. To exploit multi-modal data in the glass surface detection problem, we design the CCM module to adaptively learn the context features from both RGB and depth information.

Fig. 5 illustrates the structure of the proposed CCM module. It consists of four submodules to model the multi-modal context from different aspects. The outputs of these four submodules are concatenated for adaptive selection to produce the final cross-modal feature.

RGB Context Mining Submodule. Given the input RGB features $x_{RGB} \in \mathbb{R}^{C \times H \times W}$, this submodule extracts a series of multi-scale context features $\mathbb{C}_{r_{RGB}}^{RGB}$ by atrous convolutions with dilation rate $r \in [1, 2, 4, 8]$. These multi-scale context

features are then fused mutually by element-wise addition to form an interim rich representation of contextual information (\mathbb{RC}^{RGB}). After obtaining all permuted pairs of different context scales, these feature pairs are then concatenated to produce the aggregated rich contextual features for the RGB information \mathbb{ARC}_{RGB}^{RGB} . The whole process of this context aggregation operation is:

$$\mathbb{RC}_{r_i, r_j}^{RGB} = \mathbb{C}_{r_i}^{RGB} + \mathbb{C}_{r_j}^{RGB} (r_i < r_j), \quad (1)$$

where r_i and r_j are two different dilation rates used to produce the multi-scale context features \mathbb{C} .

The aggregated rich contextual features for the RGB information \mathbb{ARC}_{RGB}^{RGB} is then computed as:

$$\mathbb{ARC}_{RGB}^{RGB} = \text{Concat}(\underbrace{\mathbb{RC}_{1,2}^{RGB}, \mathbb{RC}_{1,4}^{RGB}, \dots, \mathbb{RC}_{2,8}^{RGB}, \mathbb{RC}_{4,8}^{RGB}}_{(4)}), \quad (2)$$

\mathbb{ARC}_{RGB}^{RGB} are then forwarded to a channel-wise attention (CNA) and a context-wise attention (CXA). The CNA mechanism that we use in the submodule consists of an average pooling layer and two convolution layers with a ReLU and sigmoid activation, as:

$$\text{CNA}(x) = x \times \sigma(\psi_2(\text{ReLU}(\psi_1(\mu(x))))), \quad (3)$$

where μ , ReLU , σ and ψ are the global average pooling (GAP) layer, ReLU, sigmoid function and convolution layers with a 1×1 kernel, respectively. ψ_1 and ψ_2 are 1×1 convolution layers with different weights. x represents the input features. The output of channel-wise attention has the

same number of channels as the input features x . Similarly, we can obtain the CXA by adjusting the output channels of the convolution layers that we use. Unlike CNA, which computes individual weights for different channels in the input features, the attention weights for the CXA are shared across all channels within the same context by squeezing and broadcasting. We finally multiply the channel-wise attention weights, the context-wise attention weights and the input features together to form the final output y^{RGB} .

Depth Context Mining Submodule. Similar to the RGB context mining submodule, we can obtain the aggregated rich contextual features for the depth information $\text{ARC}^{\text{depth}}$ by the same module design. The difference between the RGB context mining submodule and the depth context mining submodule is that the former submodule takes the RGB backbone features x^{RGB} as input, while the later submodule takes the depth backbone features x^{depth} . The model weights of these two submodules are not shared, so that they can focus on context mining in their own modalities. We also apply the channel-wise attention and the context-wise attention on $\text{ARC}^{\text{depth}}$ to produce the final output y^{depth} of this submodule.

Implicit Multi-modal Context Mining Submodule. The RGB and depth context mining submodules only consider a single-modal input. To model cross-modal contexts, we propose the implicit multi-modal context mining submodule, which aims to extract multi-modal rich contextual features implicitly by taking the fused multi-modal features as input. Specifically, this submodule takes the RGB backbone features x^{RGB} and the depth backbone features x^{depth} as input. These two input features are first concatenated and forwarded to a convolution layer to obtain the implicit multi-modal input features x^{mul} . Architecturally, this submodule has the same design as the RGB and the depth context mining submodules, and outputs implicit multi-modal rich context features ARC^{imp} . Like the first two submodules, we then apply channel-wise attention and context-wise attention on ARC^{imp} to obtain the final output y^{imp} of this submodule.

Explicit Multi-modal Context Mining Submodule. Since the implicit multi-modal context mining submodule only takes in the fused single-scale RGB and depth features and cannot disentangle multi-modal contexts in multiple scales, it is insufficient for modeling the contextual associations between different modalities. To capture the multi-modal contextual information in multiple scales explicitly, we propose the explicit multi-modal context mining submodule. Unlike the implicit one, which takes the directly fused backbone features from the RGB and depth backbone networks as input, this submodule utilizes the rich context features $\text{RC}_{r_i, r_j}^{\text{RGB}}$ and $\text{RC}_{r_i, r_j}^{\text{depth}}$ generated by the single-modal context mining submodules (*i.e.*, RGB and depth context mining submodules). Each set of rich context features from the same scale are forwarded to a 3×3 convolution with a r_j dilation rate. The aggregated rich contextual features for the explicit multi-modal rich context features ARC^{exp} are

computed as:

$$\begin{aligned} \text{RC}_{r_i, r_j}^{\text{exp}} &= \psi_{r_j}(\text{RC}_{r_i, r_j}^{\text{RGB}} + \text{RC}_{r_i, r_j}^{\text{depth}}) \\ \text{ARC}^{\text{exp}} &= \text{Concat}(\underbrace{\text{RC}_{1,2}^{\text{exp}}, \text{RC}_{1,4}^{\text{exp}}, \dots, \text{RC}_{2,8}^{\text{exp}}, \text{RC}_{4,8}^{\text{exp}}}_{\binom{4}{2}}), \end{aligned} \quad (4)$$

Finally, we forward ARC^{exp} to our channel-wise attention and the context-wise attention to obtain the final output y^{exp} of this submodule.

Adaptive Selection. Simply combining single-modal (RGB or depth) contextual features and multi-modal contextual features will cause performance drop owing to the presence of domain gap between different modalities. For example, it would be challenging to predict glass surfaces from insufficient visual information (*e.g.*, lack of context and weak reflection), while the depth information may be able to supplement this limitation. In addition, rigidly selecting a particular set of contextual information from different modalities can reduce the generality of the proposed model, as the contextual information from different modalities may differ in different cases in predicting the glass surfaces. Thus, we adaptively select the features from RGB context, depth context, implicit multi-modal context, and explicit multi-modal context information by dynamically adjusting the importance of different contextual features. To achieve this goal, we concatenate the outputs of these four context mining submodules as the input of our adaptive selection process, denoted as $x^{\text{selection}} \in \mathbb{R}^{4C \times H \times W}$. We feed $x^{\text{selection}}$ to a 1×1 convolution layer to reduce its channel size to C . After that, we apply the channel-wise attention mechanism to these features in order to capture the importance of each channel. According to the extracted channel-wise attention weights, we can adaptively select the context features by multiplying these weights to the input features to obtain the final cross-modal rich contextual features CRC as the output of the CCM module.

4.2 Depth-missing Aware Attention (DAA) Module

We observe that missing depth often appears around glass surfaces in the depth map due to light transmission, refraction and possibly reflection of the glass surface. To exploit this cue, we propose a novel DAA module to explicitly involve the spatial information of the depth-missing regions into our framework. The proposed DAA module takes the final output of the CCM module CRC , the output of the RGB context mining submodule y^{RGB} and the output of the depth context mining submodule y^{depth} in the CCM module as the input features. Besides, we also take the resized depth-missing map Dm of the same spatial resolution as the input features. Fig. 6 illustrates the structure of the proposed DAA module.

Formally, the DAA module is defined as:

$$\begin{aligned} f_k^i &= \varphi_v^i(x_i) + Dm, \\ f_{out}^i &= \gamma^i \sigma(\varphi_q^i(x_i) \varphi_k^i(x_i)^T) f_k^i + x_i, \end{aligned} \quad (5)$$

where φ_q^i , φ_k^i and φ_v^i are 1×1 convolution layers for the i modality features. σ is a softmax function. γ^i is a learnable weighting parameter for the i modality features. f_{out}^i are the output features for the i modality. We denote the $i \in \{\text{cm}, \text{RGB}, \text{depth}\}$ as the cross-modal, RGB and depth modality, respectively.

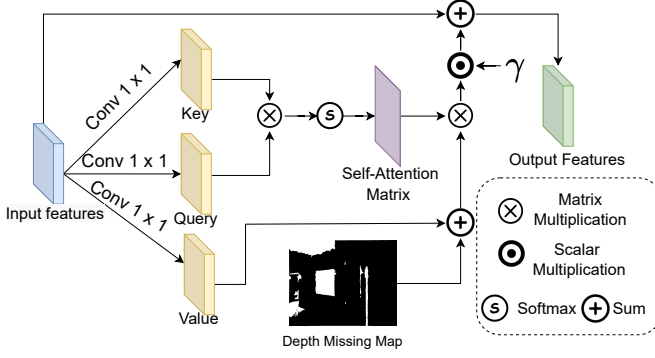


Fig. 6. Illustration of our proposed DAA module. We use three individual 1×1 convolution layers to generate key, query and value features from the input features. The key and query features are multiplied and then forwarded to a softmax operator to form the self-attention matrix. The depth missing map is added to the value features and then multiplied by the self-attention matrix and a learnable weight parameter γ to output the depth-missing enhanced features, which are further added to the input features to produce the output features of the DAA module.

4.3 Loss Functions

We use a hybrid loss function, which combines the binary cross-entropy (BCE) loss and the interaction-over-union (IoU) loss to supervise the training of the multi-scale glass surface maps. The final loss function is:

$$Loss = \sum_{i=1}^N (L_{BCE} + L_{IoU}), \quad (6)$$

where L_{BCE} and L_{IoU} are the binary cross-entropy loss and the interaction-over-union loss, respectively, between the predicted glass surfaces on the i -th stage and the ground truth glass surface map. N refers to the number of stages that we use in our framework.

5 EXPERIMENTS

5.1 Datasets and Evaluation Metrics

We conduct two sets of experiments. One set is based on using our proposed RGB-D glass surface detection dataset, and the other is based on using the two existing glass surface detection datasets, *i.e.*, [31], [41]. The first set of experiment is to evaluate how well our proposed method performs when trained/tested under our proposed setting, *i.e.*, based on RGB-D data. The second set of experiment is to evaluate how well our proposed method performs when trained/tested under the existing setting, *i.e.*, based on RGB data. For our dataset, we use 2,400 images for training and 609 images for testing. For the two existing datasets, we follow their training and test splits.

For the evaluation, we use four metrics to evaluate the performances of our methods: intersection over union (IoU), F-measure, mean absolute error (MAE), and balance error rate (BER). MAE is formulated as:

$$MAE = \frac{1}{HW} \sum_{i=1}^H \sum_{j=1}^W |P(i, j) - G(i, j)|, \quad (7)$$

where P is the predicted mask, and G is ground truth. H and W are the width and height of the input image.

TABLE 3

Quantitative comparison of our method with the state-of-the-art methods from relevant fields on our RGB-D GSD dataset. All methods are trained and tested on the training/testing splits of our dataset. Best results are shown in bold.

Methods	Venue	IoU \uparrow	$F_\beta \uparrow$	MAE \downarrow	BER \downarrow
DANet [94]	ECCV 2020	0.636	0.791	0.063	14.94
BBS-Net [10]	ECCV 2020	0.662	0.808	0.055	14.24
DCF [22]	CVPR 2021	0.655	0.803	0.058	14.12
SPNet [96]	ICCV 2021	0.706	0.831	0.050	11.41
CLNet [80]	ICCV 2021	0.707	0.829	0.051	11.00
MINet [45]	CVPR 2020	0.653	0.802	0.055	14.10
GateNet [91]	ECCV 2020	0.668	0.816	0.053	12.86
CSNet [8]	PAMI 2021	0.472	0.659	0.108	22.56
PGNet [71]	CVPR 2022	0.638	0.789	0.067	13.86
GDNet [41]	CVPR 2020	0.468	0.631	0.119	19.25
Lin <i>et al.</i> [31]	CVPR 2021	0.714	0.822	0.048	9.73
EBLNet [16]	ICCV 2021	0.707	0.819	0.048	10.91
Ours		0.742	0.853	0.043	9.33

F-measure is calculated by a weighted combination of Precision and Recall:

$$F_\beta = \frac{1 + \beta^2 (Precision \times Recall)}{\beta^2 Precision + Recall}, \quad (8)$$

where β^2 is set to 0.3 as suggested in [1].

The IoU score is calculated as:

$$IoU = \frac{N_{tp}}{N_{tp} + N_{fp} + N_{fn}}, \quad (9)$$

where N_{tp} , N_{fp} and N_{fn} are the numbers of true positive, false positive and false negative pixels, respectively.

The BER score is a widely used metric in shadow detection to measure the binary prediction from a balance-aware perspective, and is formulated as:

$$BER = 1 - 0.5 \times \left(\frac{N_{tp}}{N_p} + \frac{N_{tn}}{N_n} \right), \quad (10)$$

where N_{tp} , N_{tn} , N_p , N_n are the numbers of true positive, true negative, glass and non-glass pixels, respectively.

5.2 Implementation Details

Our proposed network is implemented using Pytorch. We use ResNext-101 [74] pretrained on ImageNet as our backbone network for the RGB input image. The details of our depth backbone network are shown in Table 2. We use the Adam optimizer [24] with an initial learning rate of $1e-4$. The initial learning rate is divided by 10 after 120 epochs. We resize all RGB images, depth maps and the corresponding ground truth masks to the spatial size of 400×400 , and then randomly crop them to 384×384 . To prevent overfitting, we adopt random horizontal flipping during our training process. We set the number of training epochs to 130, and the batch size used in training to 14. We randomly initialize the parameters in all layers except the backbone network for RGB input images. Note that we do not apply any post-processing technique (*e.g.*, conditional random field (CRF) [25]) to our predicted maps for final output. Our model takes about 14 hours to converge, and 0.10s per image for inference on a single RTX2080Ti.

TABLE 4
Quantitative results comparison of our method with the state-of-the-art RGB-based models on two existing glass surface detection datasets, GDD [41] and GSD [31]. Best results are shown in bold.

Methods	GDD (CVPR 20')				GSD (CVPR 21')			
	IoU \uparrow	$F_\beta \uparrow$	MAE \downarrow	BER \downarrow	IoU \uparrow	$F_\beta \uparrow$	MAE \downarrow	BER \downarrow
BASNet [49]	0.808	0.891	0.106	9.37	0.698	0.808	0.106	13.54
MINet [45]	0.844	0.919	0.077	7.40	0.773	0.879	0.077	9.54
GateNet [91]	0.817	0.931	0.073	8.84	0.689	0.898	0.073	10.12
CSNet [8]	0.773	0.876	0.135	11.33	0.666	0.805	0.135	14.76
PGNet [71]	0.857	0.930	0.074	6.82	0.805	0.897	0.068	7.88
MirrorNet [77]	0.851	0.903	0.083	7.67	0.742	0.828	0.090	10.76
PMD [32]	0.870	0.930	0.067	6.17	0.817	0.890	0.061	6.74
GDDNet [41]	0.814	0.909	0.097	8.83	0.790	0.869	0.069	7.72
EBLNet [16]	0.870	0.922	0.064	6.08	0.817	0.878	0.059	6.75
Lin <i>et al.</i> [31]	0.881	0.932	0.059	5.71	0.836	0.903	0.055	6.12
Ours	0.883	0.933	0.059	5.65	0.849	0.912	0.050	6.02

5.3 Quantitative Evaluation

We perform two sets of experiments to evaluate the performance of the proposed method quantitatively. In our first set of experiments, we focus on RGB-D glass surface detection on our proposed RGB-D GSD dataset. We compare the proposed method with 12 state-of-the-art methods from relevant fields on our proposed RGB-D GSD dataset. These methods include DANet [94], BBS-Net [10], DCF [22], SPNet [96], and CLNet [80] for RGB-D salient object detection; MINet [45], GateNet [91], CSNet [8] and PGNet [71] for RGB salient object detection; GDDNet [41], Lin *et al.* [31], and EBLNet [16] for RGB glass surface detection. For these baseline methods, we use their publicly available codes with default configurations. For the RGB-based methods, we only use the RGB images and the ground truth masks for training and testing. Table 3 shows the experimental results. We can see that our proposed method significantly outperforms these baseline methods on all four metrics: *i.e.*, intersection-over-union (IoU), F-measure (F_β), mean absolute error (MAE), and balance error rate (BER). In particular, our method shows substantial improvement on MAE, with a performance increase by 10.42% over the second-best method Lin *et al.* [31].

In our second set of experiments, we study how well our proposed method performs when trained and tested on the existing RGB glass surface detection datasets (*i.e.*, GDD [41] and GSD [31]), which do not contain depth information for training and evaluation. We compare our method with relevant RGB-based methods, including BASNet [49], MINet [45], GateNet [91], CSNet [8], and PGNet [71] for salient object detection; MirrorNet [77] and PMD [32] for mirror detection; GDDNet [41], EBLNet [16], and Lin *et al.* [31] for glass surface detection. We use their official codes with the default configurations for all these methods. We train and test all methods on the training/test splits of the same dataset. To adopt our method to RGB glass surface detection, we keep the RGB backbone and the RGB context mining submodule used in the CCM module, with the depth backbone network and the DAA modules removed from our original framework. Table 4 shows the experimental results. We can see that our method outperforms all compared methods on both RGB glass surface

detection datasets, GDD [41] and GSD [31], even though it does not use any auxiliary information as some glass surface detection methods do (*e.g.*, boundary labels used in [16] and the reflection maps used in [31]). Specifically, our method achieves a significant performance improvement on the more challenging GSD dataset [31]. The reason for our method to obtain a relatively minor performance gain on GDD [41] is that GDD contains images mostly captured from limited scenes and existing methods can perform very well on them. These results show that our method with RGB context mining submodules is particularly effective for glass surface detection in complex real-world scenes.

5.4 Qualitative Evaluation

We further demonstrate the performance of our method visually in Fig. 7. Due to space limitation, we compare our model with five state-of-the-art methods (including two best-performing RGB-D salient object detection methods CLNet [80] and SPNet [96], according to their performance in Table 3, and all three existing glass surface detection methods).

From the 1st and 2nd rows of Fig. 7, we can see that state-of-the-art methods may fail to accurately detect the glass regions, which may be visually ambiguous due to occlusion (the glass on the right end in the 1st row) or uncommon context (2nd row). It may be interesting to note that both RGB-D methods, CLNet [80] and SPNet [96] perform reasonably well. This demonstrates the importance of depth information in the RGB-D glass surface detection problem. In these cases, using only RGB information to predict the glass surfaces can be challenging.

From the 3rd and 4th rows, we can see that our method can correctly detect glass regions with over-exposed, through integrating both RGB and depth contextual information. However, only exploiting RGB-D information without considering the properties of glass surfaces is not reliable for glass surface detection, as demonstrated by the results from CLNet [80] and SPNet [96].

In the 5th row, both CLNet [80] and SPNet [96] can only detect the region of the glass surface with missing depth, but fail to detect the remaining part of the glass surface with depth values (near the bottom-right corner). In contrast,

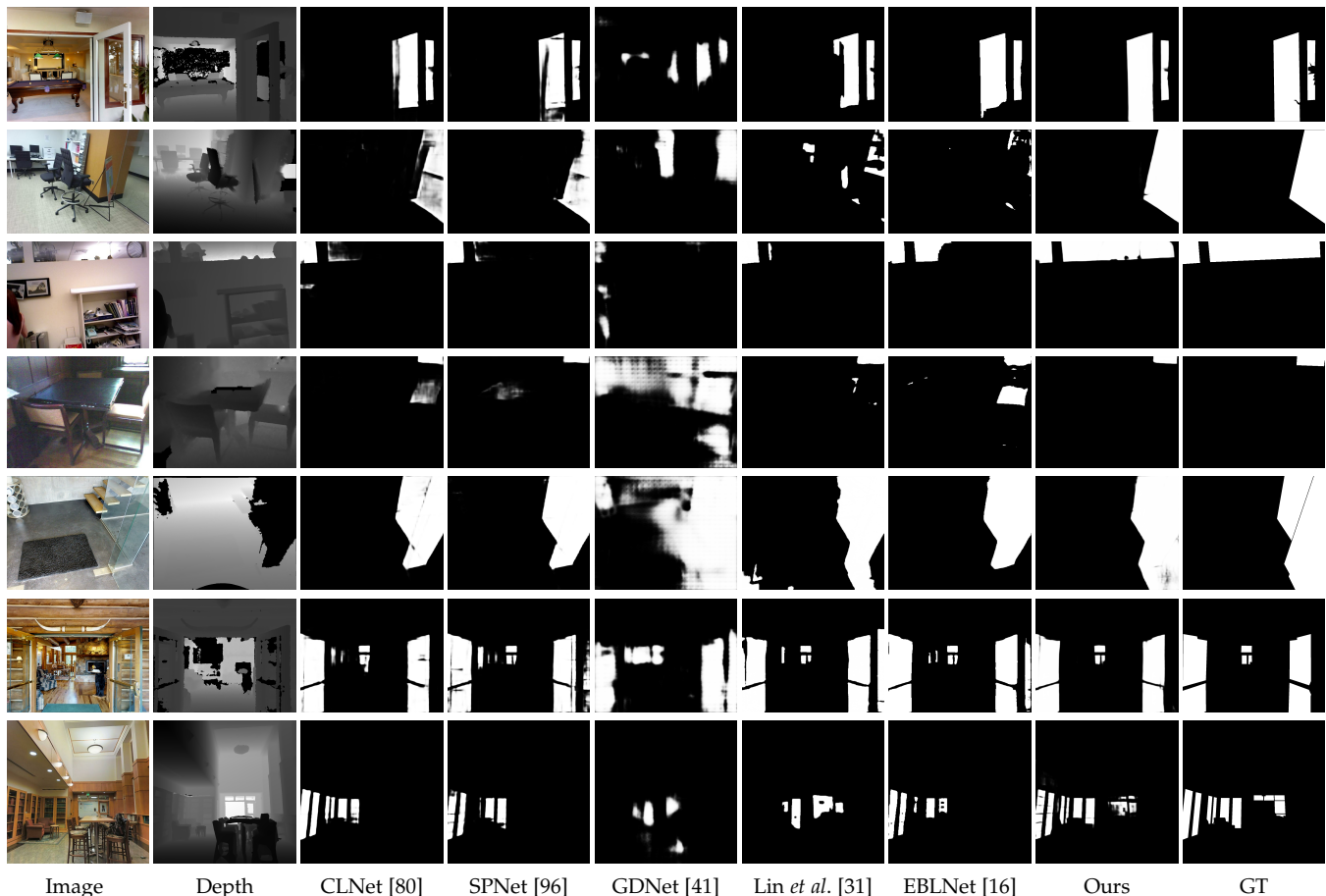


Fig. 7. Visual comparison of our method with state-of-the-art methods on images from our RGB-D GSD dataset. CLNet [80] and SPNet [96] are RGB-D salient object detection methods, while GDNet [41], Lin *et al.* [31], and EBLNet [16] are RGB-based glass surface detection methods.

with cross-modal context mining, our method can predict the full glass surface accurately.

The last two rows of Fig. 7 show two challenging examples, where the input images contain extremely small glass surface regions. Our method can still significantly outperform the other baseline methods. We attribute the superior performances of our method to the multi-scale context features incorporated in our proposed CCM module.

5.5 Ablation Study

Finally, we perform an ablation study to evaluate each of the proposed components of our model. Table 5 shows the results of our ablation study. We can see that adding either the CCM module or the DAA module helps improve the model performances, but our final model with both CCM and DAA modules performs the best on all four metrics. Note that adding the CCM modules to the base network (*i.e.*, RGB and depth backbone networks with decoders) to form an ablated model (“Base + CCM”) significantly outperforms the ablated model (“Base + DAA”) that adds the DAA module to the base network. We attribute this to the success of our cross-modal contextual mining process conducted by the CCM module, which benefits the RGB-D glass surface detection task from a global view. Figure 8 shows a visual example of the component analysis. We can see that the proposed CCM and DAA modules can

TABLE 5
Ablation study of the proposed method on the RGB-D GSD dataset. “Base” denotes the RGB and depth backbone networks with decoders, without CCM and DAA modules. “CCM” is the cross-modal context mining module. “DAA” is the depth-missing aware attention. Our final model includes both CCM and DAA. Best results are shown in bold.

Methods	IoU \uparrow	$F_{\beta}\uparrow$	MAE \downarrow	BER \downarrow
Base	0.703	0.814	0.046	11.14
Base + CCM	0.727	0.836	0.045	9.59
Base + DAA	0.706	0.819	0.046	10.48
Ours	0.742	0.853	0.043	9.33

help improve performance by removing the over-predicted regions.

Benefits of the Depth Cue. To verify the benefits of the depth cue in RGB-D glass surface detection, we conduct the following experiments: 1) removing all depth-related modules (*i.e.*, only keep the RGB backbone and the RGB context mining submodule in CCM) and then retrain the proposed network (“Ours w/ RGB only” in Table 6); 2) replacing the depth map with the grayscale image of the input RGB image during inference (“Ours w/ RGB + Gray” in Table 6); 3) replacing the depth map with a black image during inference (“Ours w/ RGB + Black” in Table 6). We can see that using only RGB information and removing depth-related modules

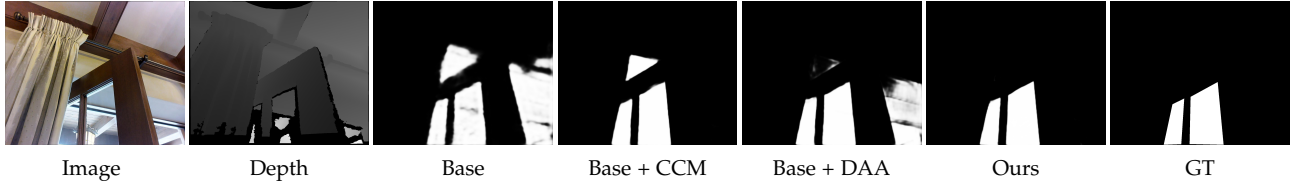


Fig. 8. A visual example of the ablation study. The Base model over-predicts the glass regions. With the CCM module, the model can largely exploit cross-modal information to reduce the over-prediction. The DAA module can also help reduce the triangular glass-like region near the center. As the region does not contain any depth missing pixels, it is less likely to be a glass surface. The full model of our method (including both CCM and DAA modules) performs the best in this example.

TABLE 6

Ablation study on the benefits of the depth cue, on our RGB-D GSD dataset. “Ours w/ RGB only” denotes the ablated model containing only the RGB backbone network and the decoders, with the depth backbone network and DAA removed. “Ours w/ RGB + Gray” is our final model but replacing the input depth map with the grayscale image of the input RGB image during inference. “Ours w/ RGB + Black” is our final model but replacing the input depth map with a black image during inference. Best results are shown in bold.

Methods	IoU \uparrow	F_β \uparrow	MAE \downarrow	BER \downarrow
Ours w/ RGB only	0.686	0.802	0.052	11.47
Ours w/ RGB + Gray	0.325	0.646	0.112	33.02
Ours w/ RGB + Black	0.352	0.639	0.112	32.87
Ours	0.742	0.853	0.043	9.33

(“Ours w/ RGB only”) produce unsatisfying results on our RGB-D GSD dataset. In addition, we also find that replacing the depth map with the grayscale version of the input image or with a black (empty) map significantly decreases the model performances. These experimental results show the effectiveness and importance of the depth cue for RGB-D glass surface detection.

Effectiveness of the CCM Module. Table 7 shows the ablation study on the proposed CCM module. Specifically, we keep all other modules in the final model while replacing our proposed CCM module with its variants, where “RGB”, “D”, “imp.”, and “exp.” refer to the RGB context mining submodule, depth context mining submodule, implicit multi-modal context mining submodule, and explicit multi-modal context mining submodule, respectively, in the CCM module. We can see that the single-modal variants (*i.e.*, “CCM w/ RGB” and “CCM w/ D”) have the worse performances, compared with the other three multi-modal variants. We also observe that the ablated models with the cross-modal context mining submodule (*i.e.*, “CCM w/ RGB + D + imp.” and “CCM w/ RGB + D + exp.”) outperform those without the submodules (*e.g.*, “CCM w/ RGB + D”). This indicates the importance of cross-modal context modeling in our CCM module. Finally, our final model performs the best among all ablated models, which shows that the CCM module with cross-modal mining can provide a great performance improvement in glass surface detection.

Effectiveness of the DAA Module. Table 8 shows the ablation study on our proposed DAA module. “DAA w/o Dm ” refers to the DAA module without taking the depth-missing map as input. We design three other ablated models: “DAA on RGB”, “DAA on Depth”, and “DAA on CM” as adopting the DAA module only on the RGB, depth, and

TABLE 7

Ablation study of the CCM module, on our RGB-D GSD dataset. “RGB”, “D”, “imp.”, and “exp.” refer to the RGB context mining submodule, depth context mining submodule, implicit multi-modal context mining submodule, and explicit multi-modal context mining submodule, respectively, in the CCM module. “CCM w/ RGB” refers to the CCM module containing only the RGB context mining submodule, while “CCM w/ RGB + D” refers to the CCM module with both RGB and depth context mining submodules.

Methods	IoU \uparrow	F_β \uparrow	MAE \downarrow	BER \downarrow
CCM w/ RGB	0.708	0.819	0.046	10.44
CCM w/ D	0.695	0.815	0.053	10.92
CCM w/ RGB + D	0.716	0.827	0.047	10.18
CCM w/ RGB + D + imp.	0.736	0.839	0.046	9.66
CCM w/ RGB + D + exp.	0.737	0.841	0.043	9.65
Ours	0.742	0.853	0.043	9.33

TABLE 8

Ablation study of the DAA module, on our RGB-D GSD dataset. “DAA w/o Dm ” refers to the DAA module without using the depth missing map as input. “DAA on RGB/Depth/CM” refers to the DAA module applied on the RGB/depth/cross-modal contextual features extracted by the preceding CCM modules in *stage4* and *stage3*. Best results are shown in bold.

Methods	IoU \uparrow	F_β \uparrow	MAE \downarrow	BER \downarrow
DAA w/o Dm	0.733	0.835	0.045	9.92
DAA on RGB	0.738	0.838	0.044	9.62
DAA on Depth	0.729	0.831	0.048	9.85
DAA on CM	0.739	0.846	0.045	9.30
Ours	0.742	0.853	0.043	9.33

cross-modal contextual features from the CCM modules, to test the effectiveness of the DAA module for extracting features in different modalities. Our final model adopts the DAA module with all three modalities. Experimental results show that the depth-missing information plays a key role in the DAA module, and our DAA module can effectively enhance the feature representation from different modalities.

6 CONCLUSION

In this paper, we have investigated the glass surface detection problem by considering the depth information. To this end, we first construct a new large-scale RGB-D glass surface detection dataset containing 3,009 images with the corresponding depth maps and annotations. This dataset covers diverse scenes with glass surfaces and can facilitate research on glass surface detection. We then propose a

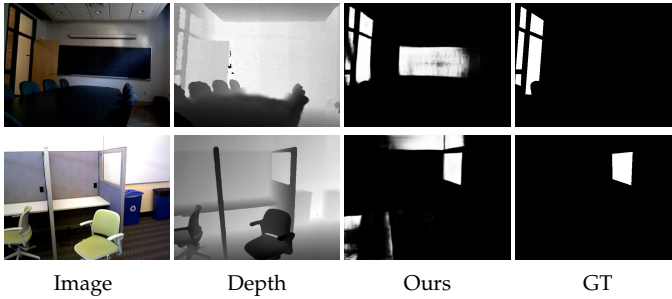


Fig. 9. Failure cases. Our method may fail when both RGB image and depth map lack contextual cues for glass surface detection.

novel RGB-D framework for glass surface detection. Our framework consists of two novel modules: (1) a cross-modal context mining (CCM) module for mining the context information among different modalities, and (2) a depth-missing aware attention (DAA) for exploiting the depth missing information around glass surfaces. Experimental results show the superior performances of our proposed framework, compared with state-of-the-art methods from relevant fields.

Despite the success, as our method focuses on mining context information in and across different modalities, it may fail if both RGB and depth information cannot provide sufficient contextual cues. Figure 9 shows that our method over-predicts glass-like regions (*i.e.*, the blackboard in the top row and the whiteboard in the bottom row) as glass surfaces, due to the lack of contextual cues in both RGB images and depth maps. As a future work, we are investigating to address the current failure cases by exploiting other cues for glass surface detection.

REFERENCES

- [1] Radhakrishna Achanta, Sheila Hemami, Francisco Estrada, and Sabine Susstrunk. Frequency-tuned salient region detection. In *CVPR*, 2009.
- [2] Edward H. Adelson and P. An. Ordinal characteristics of transparency. In *in Proc. AAAI workshop on Qualitative Vision*, pages 77–81, 1990.
- [3] I. Armeni, A. Sax, A. R. Zamir, and S. Savarese. Joint 2D-3D-Semantic Data for Indoor Scene Understanding. *ArXiv e-prints*, Feb. 2017.
- [4] Angel Chang, Angela Dai, Thomas Funkhouser, Maciej Halber, Matthias Niessner, Manolis Savva, Shuran Song, Andy Zeng, and Yinda Zhang. Matterport3d: Learning from rgb-d data in indoor environments. *International Conference on 3D Vision (3DV)*, 2017.
- [5] Hao Chen and Youfu Li. Progressively complementarity-aware fusion network for rgb-d salient object detection. In *CVPR*, June 2018.
- [6] Shuhan Chen, Xiuli Tan, Ben Wang, and Xuelong Hu. Reverse attention for salient object detection. In *ECCV*, September 2018.
- [7] Zuyao Chen, Qianqian Xu, Runmin Cong, and Qingming Huang. Global context-aware progressive aggregation network for salient object detection. *CoRR*, abs/2003.00651, 2020.
- [8] Ming-Ming Cheng*, Shanghua Gao*, Ali Borji, Yong-Qiang Tan, Zheng Lin, and Meng Wang. A highly efficient model to study the semantics of salient object detection. *IEEE TPAMI*, 2021.
- [9] Angela Dai, Angel X. Chang, Manolis Savva, Maciej Halber, Thomas Funkhouser, and Matthias Nießner. Scannet: Richly-annotated 3d reconstructions of indoor scenes. In *CVPR*, 2017.
- [10] Deng-Ping Fan, Yingjie Zhai, Ali Borji, Jufeng Yang, and Ling Shao. Bbs-net: Rgb-d salient object detection with a bifurcated backbone strategy network. In *ECCV*, 2020.
- [11] Mengyang Feng, Huchuan Lu, and Errui Ding. Attentive feedback network for boundary-aware salient object detection. In *CVPR*, June 2019.
- [12] Paul Foster, Zhenghong Sun, Jong Jin Park, and Benjamin Kuipers. Visagge: Visible angle grid for glass environments. In *2013 IEEE International Conference on Robotics and Automation*, pages 2213–2220, 2013.
- [13] Mario Fritz, Gary Bradski, Sergey Karayev, Trevor Darrell, and Michael Black. An additive latent feature model for transparent object recognition. In Y. Bengio, D. Schuurmans, J. Lafferty, C. Williams, and A. Culotta, editors, *NeurIPS*, volume 22. Curran Associates, Inc., 2009.
- [14] Chen Guo-Hua, Wang Jun-Yi, and Zhang Ai-Jun. Transparent object detection and location based on RGB-d camera. *Journal of Physics: Conference Series*, 1183:012011, mar 2019.
- [15] S. Hata, Y. Saitoh, S. Kumamura, and K. Kaida. Shape extraction of transparent object using genetic algorithm. In *Proceedings of 13th International Conference on Pattern Recognition*, volume 4, pages 684–688 vol.4, 1996.
- [16] Hao He, Xiangtai Li, Guangliang Cheng, Jianping Shi, Yunhai Tong, Gaofeng Meng, Véronique Prinet, and LuBin Weng. Enhanced boundary learning for glass-like object segmentation. In *ICCV*, pages 15859–15868, October 2021.
- [17] Qibin Hou, Ming-Ming Cheng, Xiaowei Hu, Ali Borji, Zhuowen Tu, and Philip H. S. Torr. Deeply supervised salient object detection with short connections. In *CVPR*, July 2017.
- [18] Zhiming Huang, Kaiwei Wang, Kailun Yang, Ruiqi Cheng, and Jian Bai. Glass detection and recognition based on the fusion of ultrasonic sensor and RGB-D sensor for the visually impaired. In Karin U. Stein and Ric Schleijsen, editors, *Target and Background Signatures IV*, volume 10794, pages 118 – 125. International Society for Optics and Photonics, SPIE, 2018.
- [19] Md Nazrul Islam, Murat Tahtali, and Mark Pickering. Specular reflection detection and inpainting in transparent object through mspfi. *Remote Sensing*, 13(3), 2021.
- [20] Allison Janoch. The berkeley 3d object dataset. Master’s thesis, EECS Department, University of California, Berkeley, May 2012.
- [21] Wei Ji, Jingjing Li, Shuang Yu, Miao Zhang, Yongri Piao, Shunyu Yao, Qi Bi, Kai Ma, Yefeng Zheng, Huchuan Lu, and Li Cheng. Calibrated rgb-d salient object detection. In *CVPR*, pages 9471–9481, June 2021.
- [22] Wei Ji, Jingjing Li, Shuang Yu, Miao Zhang, Yongri Piao, Shunyu Yao, Qi Bi, Kai Ma, Yefeng Zheng, Huchuan Lu, and Li Cheng. Calibrated rgb-d salient object detection. In *CVPR*, pages 9471–9481, June 2021.
- [23] Agastya Kalra, Vage Taamazyan, Supreeth Krishna Rao, Kartik Venkataraman, Ramesh Raskar, and Achuta Kadambi. Deep polarization cues for transparent object segmentation. In *CVPR*, June 2020.
- [24] Diederick P Kingma and Jimmy Ba. Adam: A method for stochastic optimization. In *ICLR*, 2015.
- [25] Philipp Krähenbühl and Vladlen Koltun. Efficient inference in fully connected crfs with gaussian edge potentials. In *NeurIPS*, 2011.
- [26] Gayoung Lee, Yu-Wing Tai, and Junmo Kim. Deep saliency with encoded low level distance map and high level features. *CVPR*, pages 660–668, 2016.
- [27] Gongyang Li, Zhi Liu, Minyu Chen, Zhen Bai, Weisi Lin, and Haibin Ling. Hierarchical alternate interaction network for rgb-d salient object detection. *IEEE TIP*, 30:3528–3542, 2021.
- [28] Gongyang Li, Zhi Liu, and Haibin Ling. Icnnet: Information conversion network for rgb-d based salient object detection. *IEEE TIP*, 29:4873–4884, 2020.
- [29] Guanbin Li and Y. Yu. Visual saliency based on multiscale deep features. In *CVPR*, pages 5455–5463, Los Alamitos, CA, USA, jun 2015. IEEE Computer Society.
- [30] Guanbin Li and Yizhou Yu. Deep contrast learning for salient object detection. In *CVPR*, June 2016.
- [31] Jiaying Lin, Zebang He, and Rynson W.H. Lau. Rich context aggregation with reflection prior for glass surface detection. In *CVPR*, 2021.
- [32] Jiaying Lin, Guodong Wang, and Rynson WH Lau. Progressive mirror detection. In *CVPR*, 2020.
- [33] Jiang-Jiang Liu, Qibin Hou, Ming-Ming Cheng, Jiashi Feng, and Jianmin Jiang. A simple pooling-based design for real-time salient object detection. In *CVPR*, June 2019.
- [34] Nian Liu and Junwei Han. Dhsnet: Deep hierarchical saliency network for salient object detection. In *CVPR*, pages 678–686, 2016.
- [35] Nian Liu, Junwei Han, and Ming-Hsuan Yang. Picanet: Learning pixel-wise contextual attention for saliency detection. In *CVPR*, June 2018.
- [36] Nian Liu, Ni Zhang, and Junwei Han. Learning selective self-mutual attention for rgb-d saliency detection. In *CVPR*, June 2020.

- [37] Tie Liu, Jian Sun, Nan-Ning Zheng, Xiaou Tang, and Heung-Yeung Shum. Learning to detect a salient object. In *CVPR*, pages 1–8, 2007.
- [38] Zhiming Luo, Akshaya Mishra, Andrew Achkar, Justin Eichel, Shaozi Li, and Pierre-Marc Jodoin. Non-local deep features for salient object detection. In *CVPR*, July 2017.
- [39] John McCormac, Ankur Handa, Stefan Leutenegger, and Andrew J. Davison. Scenenet rgb-d: Can 5m synthetic images beat generic imagenet pre-training on indoor segmentation? In *ICCV*, 2017.
- [40] K. McHenry, J. Ponce, and D. Forsyth. Finding glass. In *CVPR*, volume 2, pages 973–979 vol. 2, 2005.
- [41] Haiyang Mei, Xin Yang, Yang Wang, Yuanyuan Liu, Shengfeng He, Qiang Zhang, Xiaopeng Wei, and Rynson W.H. Lau. Don't hit me! glass detection in real-world scenes. In *CVPR*, June 2020.
- [42] H. Murase. Surface shape reconstruction of an undulating transparent object. In *ICCV*, pages 313–317, 1990.
- [43] Pushmeet Kohli, Nathan Silberman, Derek Hoiem, and Rob Fergus. Indoor segmentation and support inference from rgb-d images. In *ECCV*, 2012.
- [44] Youwei Pang, Xiaoqi Zhao, Lihe Zhang, and Huchuan Lu. Multi-scale interactive network for salient object detection. In *CVPR*, June 2020.
- [45] Youwei Pang, Xiaoqi Zhao, Lihe Zhang, and Huchuan Lu. Multi-scale interactive network for salient object detection. In *CVPR*, 2020.
- [46] Yongri Piao, Wei Ji, Jingjing Li, Miao Zhang, and Huchuan Lu. Depth-induced multi-scale recurrent attention network for saliency detection. In *ICCV*, October 2019.
- [47] Yongri Piao, Zhengkun Rong, Miao Zhang, Weisong Ren, and Huchuan Lu. A2dele: Adaptive and attentive depth distiller for efficient rgb-d salient object detection. In *CVPR*, June 2020.
- [48] Xuebin Qin, Zichen Zhang, Chenyang Huang, Chao Gao, Masood Dehghan, and Martin Jagersand. Basnet: Boundary-aware salient object detection. In *CVPR*, June 2019.
- [49] Xuebin Qin, Zichen Zhang, Chenyang Huang, Chao Gao, Masood Dehghan, and Martin Jagersand. Basnet: Boundary-aware salient object detection. In *CVPR*, 2019.
- [50] Liangqiong Qu, Shengfeng He, Jiawei Zhang, Jiandong Tian, Yandong Tang, and Qingxiong Yang. Rgb-d salient object detection via deep fusion. *IEEE TIP*, 26(5):2274–2285, 2017.
- [51] Jianqiang Ren, Xiaojin Gong, Lu Yu, Wenhui Zhou, and Michael Ying Yang. Exploiting global priors for rgb-d saliency detection. In *CVPR Workshops*, June 2015.
- [52] Viktor Seib, Andreas Barthen, Philipp Marohn, and Dietrich Paulus. Friend or foe: exploiting sensor failures for transparent object localization and classification. In *2016 International Conference on Robotics and Machine Vision*, volume 10253, pages 94–98. SPIE, 2017.
- [53] Viktor Seib, Andreas Barthen, Philipp Marohn, and Dietrich Paulus. Friend or foe: exploiting sensor failures for transparent object localization and classification. In Alexander V. Bernstein, Adrian Olaru, and Jianhong Zhou, editors, *2016 International Conference on Robotics and Machine Vision*, volume 10253, pages 94 – 98. International Society for Optics and Photonics, SPIE, 2017.
- [54] Shuran Song, Samuel P. Lichtenberg, and Jianxiong Xiao. Sun rgb-d: A rgb-d scene understanding benchmark suite. In *CVPR*, pages 567–576, 2015.
- [55] Peng Sun, Wenhui Zhang, Huanyu Wang, Songyuan Li, and Xi Li. Deep rgb-d saliency detection with depth-sensitive attention and automatic multi-modal fusion. In *CVPR*, pages 1407–1417, June 2021.
- [56] Haileleol Tibebe, Jamie Roche, Varuna De Silva, and Ahmet Kon-doz. Lidar-based glass detection for improved occupancy grid mapping. *Sensors*, 21(7):2263, Mar 2021.
- [57] Bo Wang, Quan Chen, Min Zhou, Zhiqiang Zhang, Xiaogang Jin, and Kun Gai. Progressive feature polishing network for salient object detection. *CoRR*, abs/1911.05942, 2019.
- [58] Linzhao Wang, Lijun Wang, Huchuan Lu, Pingping Zhang, and Xiang Ruan. Salient object detection with recurrent fully convolutional networks. *IEEE TPAMI*, 41(7):1734–1746, 2019.
- [59] Tiantian Wang, Ali Borji, Lihe Zhang, Pingping Zhang, and Huchuan Lu. A stagewise refinement model for detecting salient objects in images. In *ICCV*, Oct 2017.
- [60] Tao Wang, Xuming He, and Nick Barnes. Glass object segmentation by label transfer on joint depth and appearance manifolds. In *2013 IEEE International Conference on Image Processing*, pages 2944–2948, 09 2013.
- [61] Tiantian Wang, Lihe Zhang, Shuo Wang, Huchuan Lu, Gang Yang, Xiang Ruan, and Ali Borji. Detect globally, refine locally: A novel approach to saliency detection. In *CVPR*, June 2018.
- [62] Wenguan Wang, Qiuxia Lai, Huazhu Fu, Jianbing Shen, and Haibin Ling. Salient object detection in the deep learning era: An in-depth survey. *CoRR*, abs/1904.09146, 2019.
- [63] Wenguan Wang, Jianbing Shen, Ming-Ming Cheng, and Ling Shao. An iterative and cooperative top-down and bottom-up inference network for salient object detection. In *CVPR*, June 2019.
- [64] Wenguan Wang, Shuyang Zhao, Jianbing Shen, Steven C. H. Hoi, and Ali Borji. Salient object detection with pyramid attention and salient edges. In *CVPR*, June 2019.
- [65] Xun Wang and JianGuo Wang. Detecting glass in simultaneous localisation and mapping. *Robotics and Autonomous Systems*, 88:97–103, 2017.
- [66] Hao Wei, Xueen Li, Ying Shi, Bo You, and Yi Xu. Fusing sonars and lrf data to glass detection for robotics navigation. In *2018 IEEE International Conference on Robotics and Biomimetics (ROBIO)*, pages 826–831, 2018.
- [67] Hao Wei, Xue-en Li, Ying Shi, Bo You, and Yi Xu. Multi-sensor fusion glass detection for robot navigation and mapping. In *2018 WRC Symposium on Advanced Robotics and Automation (WRC SARA)*, pages 184–188, 2018.
- [68] Jun Wei, Shuhui Wang, and Qingming Huang. F3net: Fusion, feedback and focus for salient object detection. *CoRR*, abs/1911.11445, 2019.
- [69] Thomas Whelan, Michael Goesele, Steven J. Lovegrove, Julian Straub, Simon Green, Richard Szeliski, Steven Butterfield, Shobhit Verma, and Richard Newcombe. Reconstructing scenes with mirror and glass surfaces. *ACM TOG*, 37(4), July 2018.
- [70] Zhe Wu, Li Su, and Qingming Huang. Cascaded partial decoder for fast and accurate salient object detection. In *CVPR*, June 2019.
- [71] Chenxi Xie, Changqun Xia, Mingcan Ma, Zhirui Zhao, Xiaowu Chen, and Jia Li. Pyramid grafting network for one-stage high resolution saliency detection. In *CVPR*, 2022.
- [72] Enze Xie, Wenjia Wang, Wenhui Wang, Mingyu Ding, Chunhua Shen, and Ping Luo. Segmenting transparent objects in the wild. In *ECCV*, 2020.
- [73] Enze Xie, Wenjia Wang, Wenhui Wang, Peize Sun, Hang Xu, Ding Liang, and Ping Luo. Segmenting transparent object in the wild with transformer. In *IJCAI*, 2021.
- [74] Saining Xie, Ross Girshick, Piotr Dollár, Zhuowen Tu, and Kaiming He. Aggregated residual transformations for deep neural networks. In *CVPR*, 2017.
- [75] Yichao Xu, Hajime Nagahara, Atsushi Shimada, and Rin-ichiro Taniguchi. Transcut: Transparent object segmentation from a light-field image. In *ICCV*, December 2015.
- [76] Shao-Wen Yang and Chieh-Chih Wang. Dealing with laser scanner failure: Mirrors and windows. In *2008 IEEE International Conference on Robotics and Automation*, pages 3009–3015, 2008.
- [77] Xin Yang, Haiyang Mei, Ke Xu, Xiaopeng Wei, Baocai Yin, and Rynson WH Lau. Where is my mirror? In *ICCV*, 2019.
- [78] Jing Zhang, Deng-Ping Fan, Yuchao Dai, Saeed Anwar, Fate-meh Sadat Saleh, Tong Zhang, and Nick Barnes. Uc-net: Uncertainty inspired rgb-d saliency detection via conditional variational autoencoders. In *CVPR*, June 2020.
- [79] Jing Zhang, Deng-Ping Fan, Yuchao Dai, Xin Yu, Yiran Zhong, Nick Barnes, and Ling Shao. Rgb-d saliency detection via cascaded mutual information minimization. In *ICCV*, pages 4338–4347, October 2021.
- [80] Jing Zhang, Deng-Ping Fan, Yuchao Dai, Xin Yu, Yiran Zhong, Nick Barnes, and Ling Shao. Rgb-d saliency detection via cascaded mutual information minimization. In *ICCV*, 2021.
- [81] Jiaming Zhang, Kailun Yang, Angela Constantinescu, Kunyu Peng, Karin Müller, and Rainer Stiefelhagen. Trans4trans: Efficient transformer for transparent object and semantic scene segmentation in real-world navigation assistance. *CoRR*, abs/2108.09174, 2021.
- [82] Lu Zhang, Ju Dai, Huchuan Lu, You He, and Gang Wang. A bi-directional message passing model for salient object detection. In *CVPR*, June 2018.
- [83] Miao Zhang, Weisong Ren, Yongri Piao, Zhengkun Rong, and Huchuan Lu. Select, supplement and focus for rgb-d saliency detection. In *CVPR*, June 2020.
- [84] Pingping Zhang, D. Wang, Huchuan Lu, Hongyu Wang, and Xiang Ruan. Amulet: Aggregating multi-level convolutional features for salient object detection. *ICCV*, pages 202–211, 2017.
- [85] Pingping Zhang, D. Wang, Huchuan Lu, Hongyu Wang, and Baocai Yin. Learning uncertain convolutional features for accurate saliency detection. *ICCV*, pages 212–221, 2017.
- [86] Pingping Zhang, Luyao Wang, D. Wang, Huchuan Lu, and Chunhua Shen. Agile amulet: Real-time salient object detection with contextual attention. *ArXiv*, abs/1802.06960, 2018.

- [87] Xiaoning Zhang, Tiantian Wang, Jinqing Qi, Huchuan Lu, and Gang Wang. Progressive attention guided recurrent network for salient object detection. In *CVPR*, June 2018.
- [88] Jia-Xing Zhao, Yang Cao, Deng-Ping Fan, Ming-Ming Cheng, Xuan-Yi Li, and Le Zhang. Contrast prior and fluid pyramid integration for rgbd salient object detection. In *CVPR*, June 2019.
- [89] Rui Zhao, Wanli Ouyang, Hongsheng Li, and Xiaogang Wang. Saliency detection by multi-context deep learning. In *CVPR*, pages 1265–1274, 2015.
- [90] Ting Zhao and Xiangqian Wu. Pyramid feature attention network for saliency detection. In *CVPR*, June 2019.
- [91] Xiaoqi Zhao, Youwei Pang, Lihe Zhang, Huchuan Lu, and Lei Zhang. Suppress and balance: A simple gated network for salient object detection. In *ECCV*, 2020.
- [92] Xiting Zhao, Zhijie Yang, and Sören Schwertfeger. Mapping with reflection - detection and utilization of reflection in 3d lidar scans. *CoRR*, abs/1909.12483, 2019.
- [93] Xiaoqi Zhao, Lihe Zhang, Youwei Pang, Huchuan Lu, and Lei Zhang. A single stream network for robust and real-time rgb-d salient object detection. In Andrea Vedaldi, Horst Bischof, Thomas Brox, and Jan-Michael Frahm, editors, *ECCV*, 2020.
- [94] Xiaoqi Zhao, Lihe Zhang, Youwei Pang, Huchuan Lu, and Lei Zhang. A single stream network for robust and real-time rgb-d salient object detection. In *ECCV*, 2020.
- [95] Tao Zhou, Huazhu Fu, Geng Chen, Yi Zhou, Deng-Ping Fan, and Ling Shao. Specificity-preserving rgb-d saliency detection. In *ICCV*, pages 4681–4691, October 2021.
- [96] Tao Zhou, Huazhu Fu, Geng Chen, Yi Zhou, Deng-Ping Fan, and Ling Shao. Specificity-preserving rgb-d saliency detection. In *ICCV*, 2021.